Nanoscale Advances

Accepted Manuscript

This article can be cited before page numbers have been issued, to do this please use: W. D. Castro-Godoy, L. Schmidt, J. E. Argüello and A. A. Heredia, *Nanoscale Adv.*, 2026, DOI: 10.1039/D6NA00170J.

ROYAL SOCIETY OF CHEMISTRY

rsc.li/nanoscale-advances

View Article Online
DOI: 10.1039/D6NA00170J

ARTICLE

Eco-Friendly Synthesis of Silver Nanoparticles as an Unexplored Application of Photoredox Catalysis

Received 00th January 20xx,
Accepted 00th January 20xx

DOI: 10.1039/x0xx00000x

Willber D. Castro-Godoy,[a] Luciana C. Schmidt,[b] Juan E. Argüello*[c] and Adrián A. Heredia*[c]

A novel, and sustainable methodology that merges photoredox catalysis and nanotechnology for the synthesis of AgNPs is reported. This methodology employs Eosin Y as an organic photoredox catalyst under mild, aqueous, and visible-light irradiation conditions to rapidly obtain stabilized AgNPs. Optimal conditions were systematically determined, yielding AgNPs with average sizes of ca. 10 - 12 nm. A detailed reaction mechanism is also proposed, supported by experimental results and thermodynamic calculations. Furthermore, the synthesized AgNPs exhibited catalytic performance in the reduction of nitroarenes, demonstrating their potential synthetic application in organic chemistry.

Introduction

The synthesis of nanoscale metallic particles (less than 10 nm) remains a cornerstone of modern chemistry due to their unusual plasmonic properties, which allow their application in the fields of optics,[1-3] microelectronics,[4, 5] catalysis,[6-11] sensors,[12-14] data storage,[15, 16] energy conversion,[17-20] and even critical roles in biomedical challenges such as the COVID-19 pandemic,[21-27] among others.[28-30] It is well known that the size, structure, physical, chemical, and biological properties of metal nanoparticles are intrinsically ruled by the method of synthesis. Silver nanoparticles (AgNPs) can be obtained by chemical, physical, and biological methods, and given their current and growing interest, numerous reviews have summarized these methods.[31-38] The chemical reduction of metal salts in the presence of a stabilizer is the most reported chemical approach.[35] In the case of AgNPs, the most commonly used reducing agents are $NaBH_4$, citrate and ascorbate salts through a bottom-up methodology. *Photochemical methods* use light to trigger the reduction reaction and have emerged as clean versatile alternatives that offer superior spatial and temporal resolution.[39] Within this classification, *direct photo-reduction* involves solutions of metal cations irradiated with UV light, and the reduction is promoted by the protic solvents (water or alcohols) or the corresponding counterions;[40, 41] the *photosensitized reduction* relies on molecules that generate radical species under irradiation which can transfer electrons to metal cations;[42] finally, by *photocatalytic depositions*, semiconductors such as TiO_2 are used to facilitate the transfer of electrons from the conduction band to the metal cations and to deposit the new nanoparticles on the semiconductor surface.[43] Conversely, visible light-assisted photoredox catalysis is a tool that organic chemists have been intensively using over the last decade to enable chemical transformations ranging from simple reduction or oxidation reactions to challenging C-C and C-Heteroatom new bond formation.[44-48] Electronically excited photocatalysts -or their reduced or oxidized forms- are able to generate electron transfer processes that lead to the desired chemical transformations. Substrates are often organic or organometallic molecules, but there are very few examples of electron transfer from excited organic dyes to inorganic metal precursors leading to nanomaterial formation.[49-53] To date, molecular strategies have predominantly relied on synthetic organic sensitizers or specialized UV-laser systems; however, many of these approaches still present environmental drawbacks, such as the use of organic solvents or high-power energy-intensive irradiation sources. [54-57] Concurrently, while bio-inspired protocols utilizing biological extracts and light have emerged as greener alternatives,[58] they often suffer from poor kinetic control and mass-transport limitations. These biological matrices frequently lead to polydisperse particle sizes and extended reaction times, further complicated by unidentified reducing components that obscure the underlying reaction mechanisms. Consequently, developing a truly sustainable photocatalytic system that simultaneously achieves strict morphological control, rapid reaction kinetics, and mild operation conditions remains a highly desirable goal.

We have reported the reduction of Cu(II) to Cu(I) for its application in the copper-catalyzed azide-alkyne cycloaddition reaction (CuAAC) using a visible light-assisted photoredox reaction.[59] The reduction of Cu(II) to Cu(I) was possible since the photogenerated reduced form of the dye, used as a photocatalyst, was able to transfer an electron to the metal cation ($\Delta G < 0$).[60] With this in mind, we hypothesize that by carefully modifying the reaction conditions, it would be possible to achieve a full reduction to the zero-oxidation state, thereby tuning

[a] Laboratorio de Investigación en Productos Naturales (LIPN), Facultad de Química y Farmacia, Universidad de El Salvador, Final Av. de Mártires y Héroes del 30 de Julio, San Salvador 1101, El Salvador.
[b] Instituto de Tecnología Química, Universitat Politècnica de València-Consejo Superior de Investigaciones Científicas, Avda. de los Naranjos s/n, E-46022, Valencia, Spain.
[c] INFIQC-CONICET-UNC, Dpto. de Química Orgánica, Facultad de Ciencias Químicas, Universidad Nacional de Córdoba, Ciudad Universitaria, X5000HUA Córdoba, Argentina. aheredia@unc.edu.ar, juan.arguello@unc.edu.ar

the morphology, size, and physicochemical properties of the metal nanoparticles.

Herein, we present the use of eosin Y as an efficient organic photoredox catalyst for the photochemical reduction of silver ions in a completely aqueous medium, employing polyvinylpyrrolidone (PVP) as an innocuous stabilizer. In addition, the AgNPs obtained in this work are tested for the reduction of nitroarene substrates to highlight the practical advantages of this sustainable photoredox approach.

Results and discussion

Our research began by studying the optimal reaction conditions for the synthesis of AgNPs, using their optical properties as an exceptional tool to monitor the reaction progress. AgNPs, like other metal nanoparticles, present unique plasmonic properties.[61] Electromagnetic radiation can disturb electrons in the metallic nanoparticle: radiation promotes electronic oscillations around the whole nanoparticle, and as a consequence, radiation absorption occurs in certain regions of the electromagnetic spectrum. The resulting absorption spectrum depends exclusively on the nature of the metal, including shape, size, and even agglomerates or self-assembled structures.[62] Since absorption spectra provide essential information about the nature of NPs, our study focuses on the analysis of UV-vis spectra of nanoparticles obtained under different reaction conditions. During the analysis, the position and absorbance of the plasmon band -around 400 nm for AgNPs- were analyzed as well as the depression around 320 nm, which corresponds to the dielectric function imaginary component of the material.[63] The full width at half maximum (FWHM) was also studied. The FWHM value of the corresponding plasmon resonance determines the dispersion of the NPs; a large FWHM corresponds to a broad peak and, consequently, polydispersity.[64-67] This parameter is very sensitive to monodispersity; hence, narrow bands (low FWHM) are preferred when NPs are used as sensors, since small changes are rapidly detected during experiments.

The salt, $AgNO_3$, was used as the Ag(I) ion source, which is an easy-to-handle, readily available, and inexpensive metallic source; based on our previous results, eosin Y (EY) was considered the photocatalyst. Triethylamine (TEA) was used as the electron-donating sacrificial reagent. Finally, to ensure sustainable, greener conditions, water was chosen as the solvent for our study.

First, an aqueous solution of $AgNO_3$ 25 mM (0.05 mmol, 2 mL) was treated with 3 equiv. of TEA (0.15 mmol) and EY (1 mol%, 5 x 10^{-4} mmol). A brown precipitate was observed upon combining the silver salt and organic base in water, which was assigned to the oxide Ag_2O.[68] This precipitate was solubilized by continuous addition of TEA. The UV-vis spectrum of the mixture showed a band at 517 nm characteristic of EY, and an increase in the baseline due to dispersion caused by the solid (Figure 1 (a), red line). In all cases, the UV-vis spectra were acquired by taking 200 µL of the reaction mixture and transferring it to a quartz cell loaded with 3 mL of the solvent, eventually used as a blank. The mixture was purged with nitrogen for 15 minutes and irradiated with a 3 W green LED (522 nm) for 30 minutes. After irradiation, a metallic silver film was deposited on the vial, and a black suspended solid was observed (Figure 1, b). Greater scattering, the presence of EY, and a significant depression around 320 nm were observed in the UV-vis spectrum (Figure 1 (a), blue line). Under these initial conditions, no AgNPs were obtained, however, the reduction reaction was evidenced by the formation of a silver film (Figure 1, b).

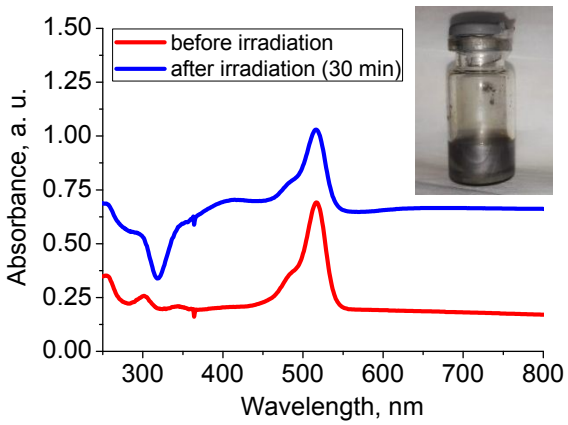

Figure 1. (a) UV-vis spectrum before (red line) and after (blue line) irradiation. (b) Photograph showing the appearance of the reaction after irradiation under initial conditions.

For now, the presence of stabilizing agents or ligands was considered for the following experiments. These are important components during the synthesis because they confine the growing material at a nanometric scale, stabilize the structure, control its shape, and prevent undesired agglomerates.[69] Firstly, mercaptosuccinic acid (MSA) was used as a ligand with a thiol group that can be covalently bind to the surface of the NPs, and it also has carboxylic acid groups exposed on the surface, producing a nanomaterial dispersible in an aqueous medium. When the MSA concentration was 1% w/v, a red precipitate and an orange suspension were obtained after 30 minutes of irradiation. In this case, the UV-vis spectrum of the supernatant showed signals at wavelengths lower than 450 nm, indicating the absence of both NPs and photocatalyst (see Figure S1 (a) in the SI). The acidic pH of the medium can protonate the photocatalyst, deactivating its photocatalytic properties. When CTAB (cetyltrimethylammonium bromide) was used as a stabilizer, a greenish-brown mixture was obtained after irradiation. The UV-vis spectrum showed a broad absorption band with a maximum at 412 nm, corresponding to AgNPs, and a narrow band of unknown origin at 236 nm (see Figure S1 (b) in the SI). The resulting solution had a translucent light-yellow appearance, typical of AgNPs suspensions. Even though AgNPs were obtained, their monodispersity was not optimal as indicated as a high FWHM value (Table S1, entry 2). The water-soluble polymers PEG200, PVA, and PVP (40 kDa and 10 kDa) were also tested as stabilizers. When PEG was used, after irradiation, a black precipitate and a fluorescent-green supernatant were obtained. The UV-vis spectrum showed the absence of any plasmonic band, but a weak signal was observed at 490 nm, probably due to partial photodecomposition of the dye under these conditions (see Figure S1 (c) in the SI). A dark suspension was obtained when PVA was used as a stabilizer. UV-vis spectrum showed a broad band around 390 nm and depression at 320 nm, consistent with the presence of metallic nanoparticulated material (Table S1, entry 4). The decomposition of the photocatalyst was also observed as a very weak band at 490 nm. The UV-vis spectrum also showed significant scattering due to the suspended material (see Figure S1 (d) in the SI).

Due to severe light scattering, reliable FWHM values could not be extracted for PVA-stabilized samples. Better results were found by using the non-toxic, inert, and biocompatible polymer PVP as a stabilizing agent. Even though PVP 10 kDa and 40 kDa were used, similar results were obtained. The reaction mixtures turned brown after irradiation, and their dilutions had a deep yellow color, typical of AgNPs suspensions. The UV-vis spectra show narrow and well-defined absorption bands around 403 nm, with a depression at 320 nm characteristic of AgNPs. After 1 h of irradiation, the resulting spectrum of the reaction mixture with PVP 10 kDa showed a shoulder around 520 nm, probably due to the remaining EY (Figure 2, red line), while in the case of PVP 40 kDa, this signal was absent, indicating the photobleaching of the photocatalyst (Figure 2, blue line). Although the results were comparable in both cases, we continued this study with PVP 40 kDa, since EY would be removed from the reaction mixture after photocatalysis was achieved.

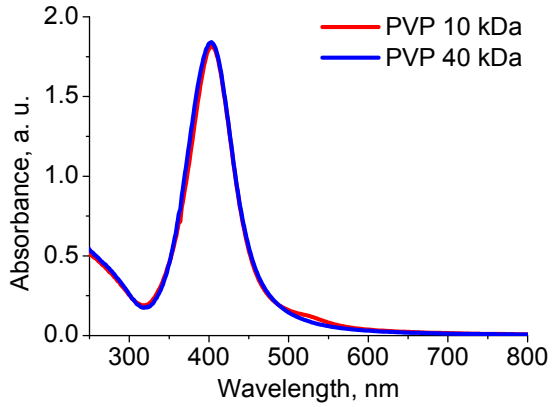

Figure 2. UV-vis spectra after irradiation employing PVP 10 kDa and PVP 40 kDa after 1 h irradiation of a mixture of $AgNO_3$ (0.05 mmol, 25 mM), TEA (3 equiv.), EY (1 mol%, 5 x 10^{-4} mmol) in 2 mL of an aqueous solution of PVP.

Next, we studied the evolution of the surface plasmon resonance band with irradiation time (Table 1 and Figure 3). The reagent mixture was then irradiated for 15 min, 30 min, 1 h, and 2 h under a nitrogen atmosphere. The presence of AgNPs was detected at each time point by observing a broad plasmonic resonance band around 410 nm which shifted to 403 nm, while the absorbance increased to a value close to 2.0 after 1 h of irradiation. The system approaches monodispersity as irradiation time increases (FWHM decreases), indicating a controlled uniform growth. Due to the few differences found between the UV-vis spectra at 1 h and 2 h, we decided to consider 1 h as the optimal reaction time.

Table 1. Irradiation reaction time study

entry	irradiation time	plasmon resonance (UV-vis spectra)	
		λ_{max} (nm)	FWHM (nm)
1	15 min	410	89
2	30 min	405	87
3	1 h	405	77
4	2 h	403	68

Reaction condition: $AgNO_3$ (0.05 mmol, 25 mM), TEA (3 equiv.), EY (1 mol%, 5 x 10^{-4} mmol) in 2 mL of an aqueous solution of PVP 40 kDa (1% w/v), under nitrogen atmosphere, irradiated with a 3 W green LED for the indicated time. Spectra were obtained from a 1:16 dilution.

Control experiments were performed, and results are shown in Table 2 and Figures 3b and 4. First, the reaction was carried out in the dark to ensure that it was assisted by visible light. In this case, the plasmon resonance of the AgNPs was absent, while the reaction mixture retained the initial color corresponding to EY (Figure 3, b).

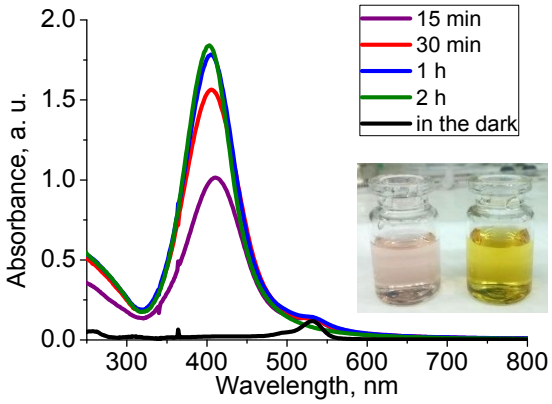

Figure 3. (a) UV-vis spectrum of the mixtures after irradiation at different reaction times. (b) Dilution (1:16) of the reaction mixtures performed in the dark (left) and under irradiated conditions (right).

Control experiments are collected in Table 2 and Figure 4. The UV-vis spectrum of the reaction in air showed a broad plasmon resonance band with a maximum at 450 nm. This spectrum is characteristic of small growing AgNPs, and oxygen from the air would slow down the growth of the first seeds (Table 2, entry 2). The formation of the AgNPs was not evident in experiments where neither base nor EY was added, and even in the absence of base (in the presence of EY) (Table 2, entries 3 and 4). However, when EY was not added, very few AgNPs were obtained after 1 h of irradiation, indicated that their formation was induced by direct irradiation in the presence of TEA as a reducing agent (Table 2, entry 5). This last experiment proved that under the same reaction conditions, the presence of an organic dye as a photocatalyst significantly accelerated the process, while an inert atmosphere improved the quality of the synthesized nanoparticles.

View Article Online DOI: 10.1039/D6NA00170J

Table 2. Control reactions.

entry	conditions	plasmon resonance (UV-vis spectra)	
		λ_{max} (nm)	FWHM (nm)
1	none	405	78
2	air atmosphere	450	279
3	without TEA and EY	ND	
4	without TEA	ND	
5	without EY	430	163

Reaction condition: $AgNO_3$ (0.05 mmol, 25 mM), TEA (3 equiv.), EY (1 mol%, 5 x 10^{-4} mmol) in 2 mL of an aqueous solution of PVP 40 kDa (1% w/v), under nitrogen atmosphere, irradiated with a 3 W green LED for 1 h. Spectra obtained from a 1:16 dilution. ND: plasmon resonance not detected.

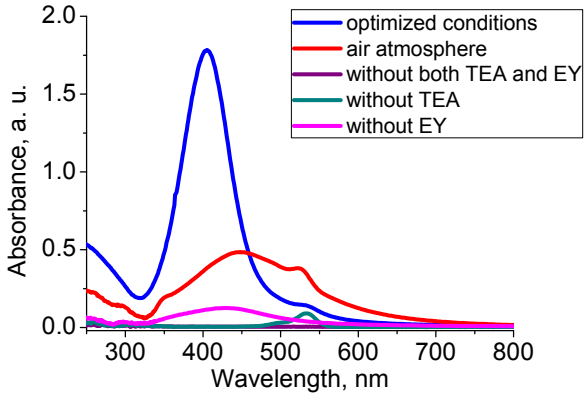

Figure 4. UV-vis spectra of reactions after irradiation under different control conditions.

Several organic dyes were also tested. The reaction conditions used are shown in Table 2, entry 1, except for the irradiation wavelength, which was selected based on the maximum absorption of each dye (Table 3 and Figure S2 in the SI). As photocatalysts, EY, rhodamine 6G (R6G), fluorescein (FL), purpurin (PP), and quinizarin (QZ) were selected, while blue, green, and red LEDs were used as the irradiation sources. The best results were obtained for EY and FL under blue LED (467 nm) irradiation (Table 3, entries 1 and 2). For PP and QZ dyes, AgNPs plasmon resonances were observed, but their intensities were low, with absorption maxima at 415 nm and 420 nm, respectively (Table 3, entries 3 and 4). The reaction with R6G showed a broad low-intensity plasmonic resonance band (Table 3, entry 4). EY, FL, R6G, and rose bengal (RB) were then tested under irradiation from a 3 W green LED (522 nm). Under these conditions, EY gives the best results (Table 3, entry 6). AgNPs from FL and RB showed a less intense and broader plasmon resonance, indicating the presence of small AgNPs (Table 3, entries 7 and 8). On the contrary, AgNPs formation was not detected when R6G was irradiated at 467 and 522 nm, as no plasmon band was observed in the 380–450 nm region, despite strong dye absorption (Table 3, entries 5 and 9). Finally, MB was used under a 3 W red LED (625 nm) irradiation without positive results (Table 3, entry 10). Although both EY and FL performed well under blue light conditions, we decided to use EY and green light as the optimal reaction conditions. Conversely, blue LED irradiation would excite the plasmon resonance of the formed AgNPs, favoring undesired reactions during synthesis; additionally, the selection of blue LED irradiation is more energetic and less selective.

Table 3. Study of dyes and LED sources.

entry	dye	LED	plasmon resonance (UV-vis spectra)	
			λ_{max} (nm)	FWHM (nm)
1	EY	blue	408	66
2	FL	blue	408	69
3	PP	blue	415	94
4	QZ	blue	420	98
5	R6G	blue	ND	
6	**EY**	**green**	**404**	**73**
7	FL	green	423	161
8	RB	green	419	118
9	R6G	green	ND	
10	MB	red	465	nd

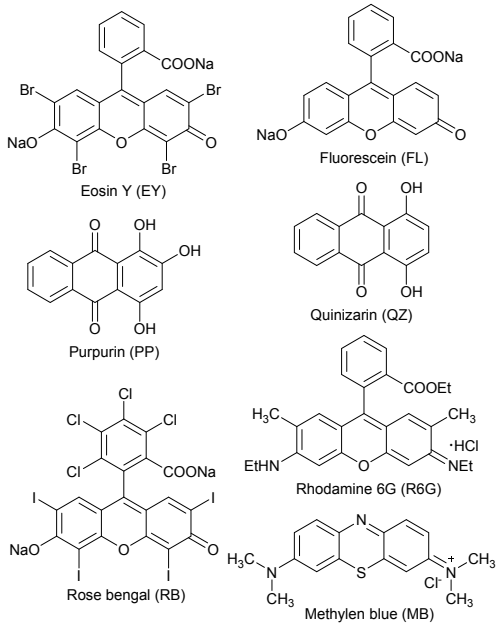

Reaction condition: $AgNO_3$ (0.05 mmol, 25 mM), TEA (3 equiv.), dye (1 mol%, 5 x 10^{-4} mmol) in 2 mL of an aqueous solution containing PVP 40 kDa, under nitrogen atmosphere, irradiated with the 3 W LED indicated in the table for 1 h. Spectra obtained from a 1:16 dilution. ND: plasmon not detected.

The optimal amount of photocatalyst was also tested. Therefore, different amounts of EY (0.1 mol%, 0.5 mol%, 1 mol%, 2 mol%, and 5 mol%) were employed (see Table S2 and Figure S3 in the SI). A weak and broad plasmon resonance was observed with EY below 1%; for higher amounts of dye, a weaker plasmon resonance was detected, while a strong absorption signal from the photocatalyst was noticed. As a result, the optimal amount of photocatalyst was 1 mol% at 1 h of irradiation time.

In addition, several electron-donating tertiary amines were also tested (Table S3 and Figure S4). The best results were obtained using TEA and DIPEA (Table S3, entries 1 and 3). Less intense and broader

plasmons were acquired using TEOA and TMEDA (Table S3, entries 2 and 4), while no plasmon resonance was detected when EDTA was used as the reducing amine. As an optimal condition, TEA was chosen as our reducing agent due to its excellent efficiency and lower cost. Finally, a series of reactions using different amounts of 40 kDa PVP was performed. The results showed well-defined and intense plasmon bands were observed in all cases (Table S4 and Figure S5). However, when PVP 40 kDa at 2% w/v was employed, a narrow intense plasmon resonance band was observed; in addition, the total absence of the dye shoulder was also noticed. An identical result was obtained for 5% w/v of PVP 40 kDa. Our findings prove that as the amount of PVP increases, the stability of the AgNPs formed improves while the decomposition of the organic photocatalyst is accelerated.[70-72] In summary, the optimal reaction conditions for the synthesis of AgNPs were $AgNO_3$ (0.05 mmol), TEA (3 equiv.), EY (1%) in 2 mL of PVP 40 kDa (2% w/v), under a nitrogen atmosphere, irradiated with a 3 W green LED for 1 h. The TEM and SEM images of the AgNPs obtained under the optimized reaction conditions showed spherical monodisperse nanoparticles with average sizes of approximately 10 nm to 12 nm (Figure 5 and Figure S7 in the SI).

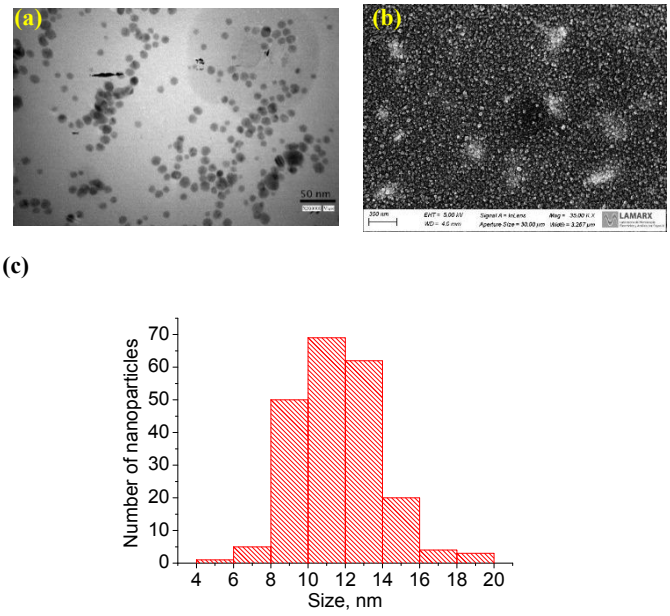

Figure 5. (a) TEM image of the synthetized AgNPs under the optimized conditions (scalebar = 50 nm). (b) SEM image of the synthetized AgNPs under the optimized conditions (scalebar = 300 nm). (c) Size distribution histogram of the photogenerated AgNPs under the optimized conditions.

The comparison between the FTIR spectrum of pure PVP and the AgNPs/PVP provides strong spectroscopic evidence for the successful surface coordination of the PVP stabilizer onto the AgNPs (Figure 6). The most significant difference lies in the redshift of the carbonyl (C=O) stretching vibration band, typically found around 1660 cm^{-1} in pure PVP (Figure 6, A); this band was observed at a lower wavenumber (1640 cm^{-1}) in the AgNPs/PVP composite (Figure 6, B). Furthermore, other characteristic absorption bands observed in pure PVP were found at 1370 cm^{-1} and 1280 cm^{-1}, corresponding to the vibration of the lactone structure and the stretching vibration of the C-N bond, respectively (Figure 6, A). The AgNPs/PVP spectrum shows changes in both the intensity and the shape of these bands (Figure 6, B). These spectral changes are attributed to the interaction between the oxygen atom of the PVP's carbonyl group, as a capping agent, and the surface of the silver nanoparticles. This coordination accounts for the mechanism of the AgNPs stabilization.

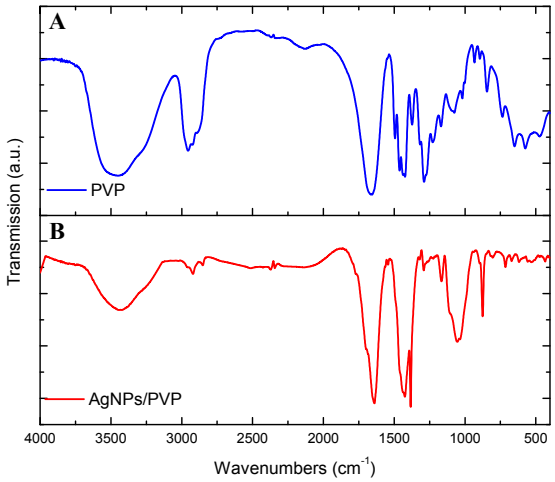

Figure 6. The FTIR spectra of (A) PVP and (B) AgNPs/PVP.

Reaction Mechanism

The collected experimental results allow us to formulate a proposed reaction mechanism (Figure 7). A photocatalyst, a tertiary amine, and visible light are essential for the photocatalyzed reduction of Ag(I) ions to Ag(0). Visible light generates electronically excited species of the photocatalyst. Thermodynamically, both singlet (^{1}PC*) and triplet (^{3}PC*) excited states could be involved in this transformation. Then, we can propose two plausible mechanisms starting from PC* (singlet (^{1}PC*) and triplet (^{3}PC*) excited states): first the *reductive quenching*, where PC* is reduced in the first step by the sacrificial reagent (Figure 7); second, *oxidative quenching*, where PC* is oxidized concomitant with the silver ions reduction (see the complete mechanism in SI). Although both mechanisms are feasible, thermodynamic calculations support that only the former allows closure of a catalytic cycle, since the latter has a strongly endergonic process as the last step. The thermodynamic calculations of excited-state electron-transfer processes, as well as thermal processes, are indicated in SI. Thus, by considering the *reductive quenching*, EY excited states (^{1}EY* or ^{3}EY*) could be reduced by TEA to generate the reduced species $EY^{\bullet-}$ and the oxidized $TEA^{\bullet+}$ ($\Delta G < 0$). Nevertheless, our previous results showed that fluorescence quenching was not observed when a solution of EY was treated with TEA. Conversely, the consumption of ^{3}EY* and concomitant formation of $EY^{\bullet-}$ were evidenced by laser flash photolysis experiments, with a quenching rate constant of 7.6 x10^6 $M^{-1}s^{-1}$.[60] Fluorescence quenching experiments were performed by monitoring the emission of EY upon the addition of silver ions, both in the presence and absence of TEA. No appreciable quenching of the EY fluorescence was observed when Ag(I) were added in the absence of TEA, confirming that ^{1}EY* does not participate in an oxidative quenching pathway (Figure S6, A). Conversely, a quenching in the fluorescence was noticed when the addition of Ag(I) was performed in the presence of TEA (Figure S6, B). Nevertheless, this quenching is static in nature, attributed to the coordination of Ag(I) to the carboxylate group of the EY, in

View Article Online DOI: 10.1039/D6NA00170J

agreement with previously reported literature data.[73] These results rule out the contribution of singlet excited state (^{1}EY*) in the operative catalytic cycle, despite its thermodynamic feasibility. From a thermodynamic point of view, the reduced photocatalyst EY$^{\bullet-}$ is reducing enough to transfer one electron to Ag(I) ion, which is reduced to a free elemental silver atom. The Ag(0) atoms will form the first nucleation points (Ag seeds) and then, stabilized AgNPs are obtained after successive reduction steps under a stabilizer-controlled growth. This last electron transfer step regenerates the photocatalyst in its fundamental initial state restarting a new cycle.

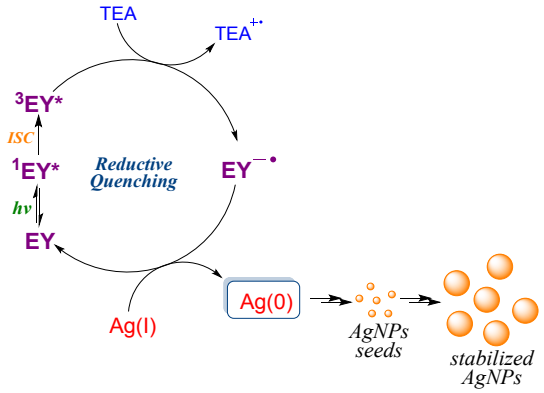

Figure 7. Proposed reaction mechanism.

Comparative analysis of AgNPs photocatalytic systems

To thoroughly contextualize the efficiency and novelty of our methodology, a comprehensive benchmarking against previously reported photochemical and photocatalytic systems for AgNPs synthesis was conducted (see Table S5). A foundational example of the use of synthetic sensitizers was reported in 2005,[54] where AgNPs (up to 20 nm) were synthesized using thionine in an organic mixture of ethanol/toluene under a high-power 250 W xenon lamp (Table S5, entry 1). More recent molecular approaches have utilized thioxanthone[55]or benzophenone derivatives (Table S5, entries 2 and 3, respectively).[57] However, these protocols still compromise environmental sustainability by relying on organic solvents such as acetonitrile, toluene or methanol, or requiring specialized laser diode equipment, while often leaving the catalytic applications of the resulting nanomaterial unexplored.

Alternatively, green synthesis protocols mediated by natural photoactive molecules or complex matrices have gained attention. For instance, a study proposed riboflavin as a metal-reduction promoter (Table S5, entry 4).[56] Nevertheless, the absence of tailored sacrificial reagents and external stabilizing agents resulted in polydisperse and significantly larger AgNPs (57–73 nm) over a prolonged irradiation time. Similarly, bio-inspired methods utilizing plant,[74-76] mushroom,[77] or yeast extracts[78] (Table S5, entries 5-8) under sunlight or white light irradiation face inherent challenges in kinetic control and particle uniformity, frequently requiring reaction times of 12–24 h or yielding large, poorly controlled colloids (up to 100 nm). Also, in these protocols, many components from the extract can act as reducing agents and stabilizers.[58, 79] The photoactive components are not properly identified, and the reaction mechanism is not adequately studied.

In contrast, our photoredox-driven system effectively bridges the gap between strict morphological control and environmental sustainability. By employing eosin Y as the photocatalyst in a completely aqueous medium, we successfully produced small, uniformly spherical AgNPs within a short reaction time and low-power green LED irradiation. Furthermore, while most reported photochemical protocols restrict their applications to antimicrobial assays or leave them unaddressed, the AgNPs obtained in this work demonstrate robust catalytic competence in the reduction of nitroarene, proving the practical synthetic utility and advantages of our sustainable approach.

Applications in Organic Synthesis

The catalytic activity of the photocatalytically-generated AgNPs was studied using the reduction reaction of nitroarenes (**1**) to anilines (**2**) in the presence of reducing agents. This reaction is important in both the laboratory and the chemical industry.[80]

First, 0.5 mmol of nitrobenzene **1a** was placed in ethanol (2 mL) at 60 °C with 6 equiv. of a reducing agent (e.g., hydrazine or $NaBH_4$). Second, the AgNPs were added directly from the reaction crude without further treatment. These reactions were performed using 1 mg of Ag (9.26 x 10^{-3} mmol, 1.8 mol%), corresponding to 150 µL of reaction crude. In the presence of AgNPs, only $NaBH_4$ reacted with **1a** to generate products (**2-4**), thus, this reducing agent was selected for the optimization of reaction conditions (Table 4). Products **2a**, **3a** and **4a** correspond to aniline, azobenzene and azoxybenzene, respectively.

Table 4. Reduction reactions of nitrobenzene (**1a**) using AgNPs

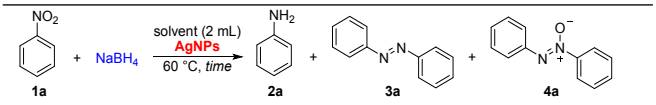

entry	solvent	AgNPs (mol%)	time (h)	**2a** (%)	**3a** (%)	**4a** (%)
1	EtOH	1.8	4	< 1	68	10
2	EtOH	1.8	24	3	87	6
3	EtOH	3.6	4	90	3	7
4	**H_2O**	**1.8**	**4**	**86**	**6**	**7**
5	H_2O	-	4	-	-	-

Reaction condition: 1a (0.5 mmol), $NaBH_4$ (6 equiv.) and AgNPs (see mol% in table) in 2 mL of solvent, under air atmosphere, stirred at 60 °C for the time shown in the table. Yields were determined by GC using the internal standard method.

When **1a** was reduced in ethanol as the solvent, the main product was azobenzene **3a** in 68% and 87% yields after 4 h and 24 h, respectively (Table 4, entries 1 and 2). The selectivity towards the amine **2a** increases when the catalyst is added at 3.6 mol% in ethanol (Table 4, entry 3) or when water is used as the solvent (Table 4, entry 4). The last condition resulted in a superior outcome since **2a** was obtained with high selectivity and in very good yield. Furthermore, water was used as a solvent, and a low catalyst load (without prior treatment) was employed. Finally, aniline was not observed in the absence of the catalyst (Table 4, entry 5).

View Article Online
DOI: 10.1039/D6NA00170J

Other nitroarenes were used to explore the scope and limitations of this new methodology. Unfortunately, not all nitro compounds tested gave good yields under the same optimized conditions for **1a**. The reaction scope obtained for compounds **1a-e** is shown in Scheme 1. The reaction conditions optimized for each nitroarene are shown between parentheses (loading of AgNPs and reaction time), where a complete conversion of the substrate was observed.

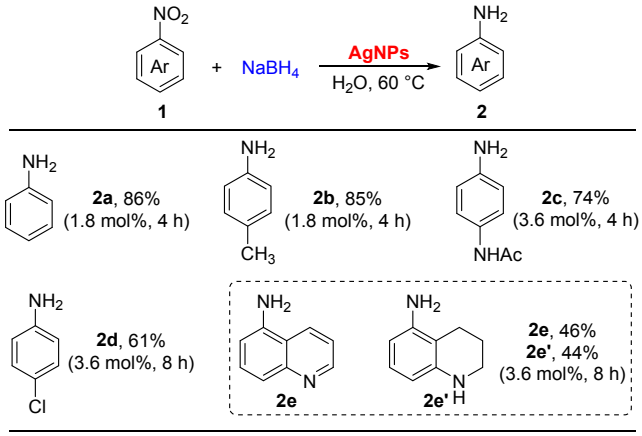

Scheme 1. Reduction reactions of nitroarenes using AgNPs.

Thus, *p*-toluidine (**2b**) was obtained in 85% yield using 4-nitrotoluene and 1.8 mol% of AgNPs after 4 h at 60 °C. On the other hand, 4-aminoacetanilide (**2c**) was produced in 74% yield when 4-nitroacetanilide was used, employing 3.6 mol% of AgNPs after 4 h. The nitroarene bearing a chlorine atom in the *para* position is less reactive, as 3.6 mol% of AgNPs and 8 h of reaction time were required to achieve complete conversion, yielding 61% of the corresponding chloroaniline **2d**. Finally, when 5-nitroquinoline was used as the starting material, it was also necessary to increase the catalyst loading and reaction time to 3.8 mol% and 8 h, respectively. Two reduction products were observed: 5-aminoquinoline (**2e**) and 5-amino-1,2,3,4-tetrahydroquinoline (**2e'**) in 46% and 44% yields, respectively. This result suggests that the photogenerated nanocatalyst can promote not only nitro group reduction but also partial hydrogenation of heteroaromatic rings.

The results of this study demonstrate the catalytic activity of AgNPs produced via photocatalysis. The model reaction of the catalytic reduction of nitro groups to the corresponding amine yields very promising results. The reaction mechanism for the reduction of nitro groups on metal nanoparticle surfaces is well establishe[81, 82] and is shown in Scheme S2. This methodology avoids the need to isolate and purify the nanocatalyst, and the studied reaction was found to be not sensitive to the remaining dye or stabilizer. Furthermore, the presence of AgNPs was detected by UV-vis both before and after the reduction reaction (Figure S6), demonstrating their high stability under strongly reducing conditions and moderate temperatures. These findings suggest that AgNPs are promising catalysts for other reactions of interest in organic synthetic chemistry. Furthermore, unlike most reported photochemical protocols where the synthetic utility of the resulting nanomaterial remains unexplored or limited to antimicrobial assays, the AgNPs obtained in this work demonstrate robust catalytic competence and excellent chemoselectivity in the reduction of nitroarene substrates, highlighting the practical advantages of this sustainable photoredox approach.

In conclusion, we were able to successfully carry out the photoreduction of Ag(I) ions using organic dyes and visible light, which led to the formation of well-stabilized AgNPs with excellent plasmonic and morphological properties. This represents one of the first examples of photoredox catalysis being employed for the synthesis of nanometric materials under mild and entirely sustainable conditions, using water as an environmentally benign and non-toxic solvent, and PVP as an eco-compatible stabilizer. Furthermore, the catalytic activity of these AgNPs was demonstrated by studying the reduction reactions of nitroarenes and the hydrogenation of heteroaromatic rings.

Experimental

General methods. ^{1}H and ^{13}C NMR spectra were recorded at 400.16 and 100.62 MHz, respectively on a Bruker 400 spectrometer, and all spectra were reported in δ (ppm) relative to Me_4Si, with $CDCl_3$ as a solvent. Gas chromatographic analyses were performed on a chromatograph with a flame-ionization detector, using a 30 m capillary column of a 0.32 mm x 0.25 µm film thickness, with a 5% phenylpolysiloxane phase. GC-MS analyses were performed on a spectrometer employing a 30 m x 0.25 mm x 0.25 µm and a 5% phenylpolysiloxane phase column. Ionization was achieved by electronic impact (70eV) and the detection setup in positive mode.

Chemicals. Ultrapure water was used without further purification. The reagents $AgNO_3$, mercaptosuccinic acid (MSA), cetyltrimethylammonium bromide (CTAB), PEG200, PVA and PVP (10 kDa and 40 kDa) were all commercial samples used without further purification. The photocatalyst eosin Y disodium salt (EY), fluorescein (FL), rose bengal (RB), rhodamine 6G (R6G), purpurin (PP), quinizarin (QZ) and methylene blue (MB) were all high-purity commercial samples used without further purification. The tertiary amines triethylamine (TEA), triethanolamine (TEOA), *N*,*N*-diisopropylethylamine (DIPEA), *N*,*N*,*N*′,*N*′-tetramethylethylenediamine (TMEDA) and ethylenediaminetetraacetic acid (EDTA) were all high-purity commercial samples used without further purification.

General experimental procedure for the synthesis of stabilized AgNPs (optimized condition). The reaction was carried out in a 10 mL glass vial, equipped with a rubber septum and a magnetic stirrer. $AgNO_3$ (8.5 mg, 0.05 mmol), TEA (15.2 mg, 20.9 µL, 3 equiv.) and 100 µL of an aqueous solution of EY 5 mM (1 mol%) were dissolved in 2 mL of a PVP 40 kDa solution at 2% w/v. The mixture was bubbled with nitrogen for 15 min. The reaction was irradiated with a 3 W green-LED (522 nm) and stirred under nitrogen atmosphere for 1 h. Then, for characterization, a sample (200 µL) was dissolved in 3 mL of the stabilized solution, and the UV-vis spectrum was acquired. The full width at half maximum (FWHM) of UV-VIS spectra was calculated by Lorentzian fitting (from 350 nm to 550 nm), where FWHM = *w* in $\frac{2A}{\pi}\left(\frac{w}{4(\lambda-\lambda_0)^2+w^2}\right)$.

General experimental procedures for the reduction of nitrobenzene (1a) using AgNPs. The reactions were carried out in a 10 mL Schlenk tube, equipped with a magnetic stirrer. The tube was charged with water (2.0 mL). Nitroarene (**1**, 0.5 mmol), $NaBH_4$ (6 equiv.) and 150 µL or 300 µL of crude of AgNPs (corresponding to 1.8 or 3.6 mol%, respectively, see Scheme 1) were added and stirred at 60 °C for 4 or

8 h (see Scheme 1). The reaction mixture was cooled to room temperature. Diethyl acetate (15 mL) and water (15 mL) were added, and the mixture was stirred. The organic layer was separated, and the aqueous layer was extracted with diethyl ether (2 × 15 mL). The combined organic extract was dried over anhydrous Na_2SO_4, and the product was isolated by column chromatography (silica gel, eluent: hexane/ethyl acetate). The identities of all the products were confirmed by ^1H, ^{13}C and GCMS, and the spectroscopic data agreed with those previously reported in the literature.

Spectroscopic data of synthesized anilines (2)

Aniline (2a).[83] ^1H NMR (400 MHz, $CDCl_3$): δ = 7.14 (td, *J* = 7.5, 3.7 Hz, 2H), 6.75 (td, *J* = 7.4, 1.0 Hz, 1H), 6.66 (dd, *J* = 7.5, 1.0 Hz, 2H), 3.60 (s, 2H). ^{13}C NMR (100 MHz, $CDCl_3$): δ = 146.5, 129.4, 118.6, 115.2. MS (EI): m/z (%) = 93 (100) $[M]^+$, 66 (48).

***p*-toluidine (2b).**[84] ^1H NMR (400 MHz, $CDCl_3$): δ = 6.96 (d, *J* = 8.1 Hz, 2H), 6.61 (d, *J* = 8.1 Hz, 2H), 3.52 (s, 2H), 2.24 (s, 3H). ^{13}C NMR (100 MHz, $CDCl_3$): δ = 143.9, 129.9, 127.9, 115.4, 20.6. MS (EI): m/z (%) = 107 (68) $[M]^+$, 106 (100), 79 (15).

4-aminoacetanilide (2c).[84] ^1H NMR (400 MHz, Acetone-d6): δ = 7.31 (d, *J* = 8.8 Hz, 2H), 6.59 (d, *J* = 8.8 Hz, 2H), 4.44 (s, 2H), 2.00 (s, 3H). ^{13}C NMR (100 MHz, Acetone-d6): δ = 168.0, 145.3, 130.5, 121.6, 115.1, 24.0. MS (EI): m/z (%) = 108 (100) $[M]^+$, 107 (40), 81 (18), 80 (41).

4-chloroaniline (2d).[83] ^1H NMR (400 MHz, $CDCl_3$): δ = 7.09 (d, *J* = 8.6 Hz, 2H), 6.60 (d, *J* = 8.6 Hz, 2H), 3.64 (s, 2H). ^{13}C NMR (100 MHz, $CDCl_3$): δ = 145.1, 129.2, 123.3, 116.4. MS (EI): m/z (%) = 127 (100) $[M]^+$, 100 (12), 92 (15).

5-aminoquinoline (2e).[85] ^1H NMR (400 MHz, $CDCl_3$): δ = 8.89 (dd, *J* = 4.1, 1.4 Hz, 1H), 8.18 (d, *J* = 8.5 Hz, 1H), 7.57 (d, *J* = 8.4 Hz, 1H), 7.51 (t, *J* = 7.5 Hz, 1H), 7.34 (dd, *J* = 8.5, 4.2 Hz, 1H), 6.82 (d, *J* = 7.3 Hz, 1H), 4.21 (s, 2H). ^{13}C NMR (100 MHz, $CDCl_3$): δ = 150.4, 149.3, 142.4, 130.1, 129.6, 120.3, 119.7, 118.9, 110.1. MS (EI): m/z (%) = 144 (100) $[M]^+$, 117 (44), 90 (25).

5-amino-1,2,3,4-tetrahydroquinoline (2e').[86] ^1H NMR (400 MHz, $CDCl_3$): δ = 6.81 (t, *J* = 7.9 Hz, 1H), 6.09 (dd, *J* = 7.8, 1.0 Hz, 1H), 6.01 (d, *J* = 7.9 Hz, 1H), 3.58 (s, 3H), 3.28 – 3.20 (m, 2H), 2.48 (t, *J* = 6.6 Hz, 2H), 2.05 – 1.97 (m, 2H). ^{13}C NMR (100 MHz, $CDCl_3$): δ = 145.8, 144.9, 127.0, 106.8, 105.6, 104.7, 41.4, 22.3, 21.5. MS (EI): m/z (%) = 148 (100) $[M]^+$, 147 (75), 145 (14), 132 (27), 93 (20).

Conclusions

We were able to successfully carry out the photoreduction of Ag(I) ions using organic dyes and visible light, which led to the formation of well-stabilized AgNPs with excellent plasmonic and morphological properties. This represents one of the first examples of photoredox catalysis being employed for the synthesis of nanometric materials under mild and entirely sustainable conditions, using water as an environmentally benign and non-toxic solvent, and PVP as an eco-compatible stabilizer. Furthermore, the catalytic activity of these AgNPs was demonstrated by studying the reduction reactions of nitroarenes and the hydrogenation of heteroaromatic rings.

Author contributions

Conceptualization: W.D.C.-G., A.A.H., L.C.S. and J.E.A.
Formal analysis: W.D.C.-G., A.A.H., L.C.S. and J.E.A.
Funding acquisition: A.A.H. and J.E.A.
Investigation: W.D.C.-G., A.A.H. and J.E.A.
Methodology: W.D.C.-G., A.A.H. and J.E.A.
Project administration: A.A.H. and J.E.A.
Resources: A.A.H. and J.E.A.
Supervision: A.A.H. and J.E.A.
Validation: A.A.H. and J.E.A.
Visualization: W.D.C.-G., A.A.H. and J.E.A.
Writing – original draft: A.A.H. and J.E.A.
Writing – review & editing: W.D.C.-G., A.A.H., L.C.S. and J.E.A.

Conflicts of interest

There are no conflicts to declare

Data availability

The data supporting this article has been included as part of the supplementary information (SI).
Supplementary information: Spectroscopic studies of stabilizers, amount of photocatalyst, sacrificial electron donors, thermodynamic studies and copies of ^1H and ^{13}C NMR spectra of synthesized anilines (2). See DOI: DOI: 10.1039/x0xx00000x

Acknowledgements

We appreciate the financial support from Consejo Nacional de Investigaciones Científicas y Técnicas (CONICET), Secretaría de Ciencia y Tecnología de la Universidad Nacional de Córdoba (SeCyT–UNC) and Secretaría de Ciencia, Tecnología e Innovación Productiva, Argentina. W. D. C-G. gratefully acknowledges the receipt of a fellowship from CONICET.

Notes and references

[1] T. Allsop, R. Neal, *Sensors,* 2019, **19**, 4874-4892.
[2] A. K. Sharma, A. K. Pandey, B. Kaur, *Opt. Fiber Technol.,* 2018, **43**, 20-34.
[3] K. Abdali, E. Al-Bermany, K. H. Abass, *J. Polym. Res.,* 2023, **30**, 138.
[4] R. J. Martín-Palma, J. Martínez-Duart, *Nanotechnology for Microelectronics and Photonics* Elsevier, Edinburgh, UK, **2017**.
[5] R. Cai, C. Liang, Y. Duan, Z. Zhao, X. Zhang, P. He, J. Yang, W.-Y. Lai, J. Wei, L. Tian, *FlexMat,* 2025, **2**, 225-283.
[6] A. Gelle, T. Jin, L. de la Garza, G. D. Price, L. V. Besteiro, A. Moores, *Chem. Rev.,* 2020, **120**, 986-1041.
[7] K. H. Leong, A. A. Aziz, L. C. Sim, P. Saravanan, M. Jang, D. Bahnemann, *Beilstein J. Nanotechnol.,* 2018, **9**, 628-648.
[8] H. Liu, J. Guan, X. Mu, G. Xu, X. Wang, X. Chen, in *Encyclopedia of Physical Organic Chemistry* (Ed.: Z. Wang), John Wiley & Sons, Hoboken, New Jersey, **2017**.
[9] D. Iordanidou, T. Zarganes-Tzitzikas, C. G. Neochoritis, A. Domling, I. N. Lykakis, *ACS omega,* 2018, **3**, 16005-16013.
[10] L. Shaker Ardakani, A. Surendar, L. Thangavelu, T. Mandal, *Synth. Commun.,* 2021, **51**, 1516-1536.
[11] S. Weiqin, Y. Qing, W. Jian, *Current Organic Chemistry,* 2011, **15**, 3692-3705.
[12] N. Ismillayli, S. Suprapto, E. Santoso, R. E. Nugraha, H. Holilah, H. Bahruji, A. A. Jalil, D. Hermanto, D. Prasetyoko, *RSC Adv.,* 2024, **14**, 6815-6822.
[13] I. Ivanišević, *Sensors,* 2023, **23**, 3692.
[14] G. Nemeth, J. Speers, S. Shaheen, V. Kitaev, in *Molecules, Vol. 30*, **2025**, p. 4745.

[15]S. Fu, X. Zhang, Q. Han, S. Liu, X. Han, Y. Liu, *Sci. Rep.,* 2016, **6**, 36701.
[16]M. Mansuripur, A. R. Zakharian, A. Lesuffleur, S.-H. Oh, R. J. Jones, N. C. Lindquist, H. Im, A. Kobyakov, J. V. Moloney, *Opt. Express,* 2009, **17**, 14001-14014.
[17]W. Ye, R. Long, H. Huang, Y. Xiong, *J. Mat. Chem. C,* 2017, **5**, 1008-1021.
[18]S. V. Boriskina, H. Ghasemi, G. Chen, *Mater. Today,* 2013, **16**, 375-386.
[19]C. Xiong, Q. Zhou, *Nanomaterials,* 2024, **14**.
[20]Y. Liu, H. Guo, X. Niu, H. Ren, Y. Hao, L. Peng, W. Yang, *ACS App. Nano Mater.,* 2025, **8**, 17504-17517.
[21]R. Medhi, P. Srinoi, N. Ngo, H.-V. Tran, T. R. Lee, *ACS Appl. Nano Mater.,* 2020, **3**, 8557-8580.
[22]R. Vazquez-Munoz, J. L. Lopez-Ribot, *Challenges,* 2020, **11**, 15.
[23]S. S. Jeremiah, K. Miyakawa, T. Morita, Y. Yamaoka, A. Ryo, *Biochem. Biophys. Res. Commun.,* 2020, **533**, 195-200.
[24]G. Ibrahim Fouad, *Bull. Natl. Res. Cent.,* 2021, **45**, 36.
[25]G. Nikaeen, S. Abbaszadeh, S. Yousefinejad, *Nanomedicine (London, England),* 2020, **15**, 1501-1512.
[26]F. Pilaquinga, J. Morey, M. Torres, R. Seqqat, M. L. N. Piña, *Wiley Interdiscip. Rev. Nanomed. Nanobiotechnol.,* 2021, **13**, e1707.
[27]S. Talebian, G. G. Wallace, A. Schroeder, F. Stellacci, J. Conde, *Nat. Nanotechnol.,* 2020, **15**, 618-621.
[28]J. Krajczewski, K. Kołątaj, A. Kudelski, *RSC Adv.,* 2017, **7**, 17559-17576.
[29]S. H. Lee, B. H. Jun, *Int. J. Mol. Sci.,* 2019, **20**, 865-887.
[30]S. Hosny, G. A. Gaber, M. S. Ragab, M. A. Ragheb, M. Anter, L. Z. Mohamed, *Arabian Journal for Science and Engineering,* 2025.
[31]B. Khodashenas, H. R. Ghorbani, *Arab. J. Chem.,* 2019, **12**, 1823-1838.
[32]H. D. Beyene, A. A. Werkneh, H. K. Bezabh, T. G. Ambaye, *Sust. Mat. Techn.,* 2017, **13**, 18-23.
[33]D. Sharma, S. Kanchi, K. Bisetty, *Arabian J. Chem.,* 2019, **12**, 3576-3600.
[34]S. Ahmad, S. Munir, N. Zeb, A. Ullah, B. Khan, J. Ali, M. Bilal, M. Omer, M. Alamzeb, S. M. Salman, S. Ali, *Int. J. Nanomedicine,* 2019, **14**, 5087-5107.
[35]N. L. Pacioni, C. D. Borsarelli, V. Rey, A. V. Veglia, in *Silver Nanoparticle Applications* (Ed.: E. I. Alarcon), Springer, Switzerland, **2015**, pp. 13-46.
[36]N. Chouhan, in *Silver Nanoparticles - Fabrication, Characterization and Applications* (Ed.: K. Maaz), IntechOpen, **2018**, pp. 21-57.
[37]K. M. F. Hasan, L. Xiaoyi, Z. Shaoqin, P. G. Horváth, M. Bak, L. Bejó, G. Sipos, T. Alpár, *Heliyon,* 2022, **8**, e12322.
[38]N. Jara, N. S. Milán, A. Rahman, L. Mouheb, D. C. Boffito, C. Jeffryes, S. A. Dahoumane, in *Molecules, Vol. 26*, **2021**, p. 4585.
[39]M. Sakamoto, M. Fujistuka, T. Majima, *J. Photochem. Photobiol. C: Photochem. Rev.,* 2009, **10**, 33-56.
[40]H. Hada, Y. Yonezawa, A. Yoshida, A. Kurakake, *J. Phys. Chem.,* 1976, **80**, 2728-2731.
[41]K. Moore Tibbetts, B. Tangeysh, J. H. Odhner, R. J. Levis, *J. Phys. Chem. A,* 2016, **120**, 3562-3569.
[42]K. L. McGilvray, M. R. Decan, D. Wang, J. C. Scaiano, *J. Am. Chem. Soc.,* 2006, **128**, 15980-15981.
[43]B. Kraeutler, A. J. Bard, *J. Am. Chem. Soc.,* 1978, **100**, 4317-4318.
[44]B. König, *Eur. J. Org. Chem.,* 2017, **2017**, 1979-1981.
[45]Y. Du, R. M. Pearson, C. H. Lim, S. M. Sartor, M. D. Ryan, H. Yang, N. H. Damrauer, G. M. Miyake, *Chem. Eur. J.,* 2017, **23**, 10962-10968.
[46]D. A. Nicewicz, T. M. Nguyen, *ACS Catal.,* 2014, **4**, 355-360.
[47]N. A. Romero, D. A. Nicewicz, *Chem. Rev.,* 2016, **116**, 10075-10166.
[48]F. Dumur, J. Lalevée, *Catalysts,* 2024, **14**, 26.
[49]J. G. Mayans, J. S. Suppo, A. M. Echavarren, *Org. Lett.,* 2020, **22**, 3045–3049.
[50]S. C. Ritter, B. Konig, *Chem. Commun.,* 2006, 4694-4696.
[51]P. Kumar, C. Joshi, A. K. Srivastava, P. Gupta, R. Boukherroub, S. L. Jain, *ACS Sustainable Chem. Eng.,* 2015, **4**, 69-75.
[52]M. D. Hardy, D. Konetski, C. N. Bowman, N. K. Devaraj, *Org. Biomol. Chem.,* 2016, **14**, 5555-5558.
[53]S. Dutta, J. E. Erchinger, F. Schäfers, A. Das, C. G. Daniliuc, F. Glorius, *Angew. Chem., Int. Ed.,* 2022, **61**, e202212136.
[54]P. K. Sudeep, P. V. Kamat, *Chem. Mater.,* 2005, **17**, 5404-5410.
[55]J.-P. Malval, M. Jin, L. Balan, R. Schneider, D.-L. Versace, H. Chaumeil, A. Defoin, O. Soppera, *J. Phys. Chem. C* 2010, **114**, 10396-10402.
[56]Z. Anwar, S. A. Ali, M. R. Shah, F. Ahmed, A. Ahmed, U. Ijaz, H. Afzal, S. Ahmed, M. A. Sheraz, M. Usmani, I. Ahmad, *J. Mol. Struct.,* 2023, **1289**, 135863.
[57]A. S. Alnafisah, E. Alqrairy, H. Tar, F. M Alminderej, L. M. Aroua, B. Graff, J. Lalevee, *ACS omega,* 2023, **8**, 3207-3220.
[58]S. Shahzadi, S. Fatima, Q. ul ain, Z. Shafiq, M. R. S. A. Janjua, *RSC Adv.,* 2025, **15**, 3858-3903.
[59]W. D. Castro-Godoy, A. A. Heredia, L. C. Schmidt, J. E. Argüello, *RSC Adv.,* 2017, **7**, 33967-33973.
[60]R. Martínez-Haya, A. A. Heredia, W. D. Castro-Godoy, L. C. Schmidt, M. L. Marin, J. E. Argüello, *J. Org. Chem.,* 2021, **86**, 5832-5844.
[61]Y. Hang, A. Wang, N. Wu, *Chem. Soc. Rev.,* 2024, **53**, 2932-2971.
[62]C. S. S. R. Kumar, *UV-VIS and Photoluminescence Spectroscopy for Nanomaterials Characterization*, Springer, Heidelberg, Germany, **2013**.
[63]S. Marhaba, in *Noble and Precious Metals - Properties, Nanoscale Effects and Applications* (Eds.: M. Seehra, A. Bristow), IntechOpen, London, UK, **2018**.
[64]S. Agnihotri, S. Mukherji, S. Mukherji, *RSC Adv.,* 2014, **4**, 3974-3983.
[65]J. P. Oliveira, A. R. Prado, W. J. Keijok, M. R. N. Ribeiro, M. J. Pontes, B. V. Nogueira, M. C. C. Guimarães, *Arab. J. Chem.,* 2020, **13**, 216-226.
[66]R. Desai, V. Mankad, S. K. Gupta, P. K. Jha, *Nanosci. Nanotechnol. Lett.,* 2012, **4**, 30-34.
[67]A. W. Orbaek, M. M. McHale, A. R. Barron, *J. Chem. Educ.,* 2014, **92**, 339-344.
[68]O. A. D. Gallardo, R. Moiraghi, M. A. Macchione, J. A. Godoy, M. A. Pérez, E. A. Coronado, V. A. Macagno, *RSC Adv.,* 2012, **2**, 2923-2929.
[69]H. Kang, J. T. Buchman, R. S. Rodriguez, H. L. Ring, J. He, K. C. Bantz, C. L. Haynes, *Chem. Rev.,* 2019, **119**, 664-699.
[70]V. K. Vidhu, D. Philip, *Micron,* 2014, **56**, 54-62.
[71]K. Jyoti, A. Singh, *J. Genet. Eng. Biotechnol.,* 2016, **14**, 311-317.

View Article Online
DOI: 10.1039/D6NA00170J

[72]A. A. Fairuzi, N. N. Bonnia, R. M. Akhir, M. A. Abrani, H. M. Akil, *IOP Conf. Ser. Earth. Environ. Sci. ,* 2018, **105**, 12-18.
[73]J. Wang, L. Chen, Y. Li, W. Shen, M. Manley-Harris, *Microchem. J.,* 2024, **196**, 109588.
[74]A. A. Alshehri, M. A. Malik, in *Biomolecules, Vol. 10*, **2020**, p. 1604.
[75]R. W. Raut, V. D. Mendhulkar, S. B. Kashid, *J. Photochem. Photobiol. B: Biol.,* 2014, **132**, 45-55.
[76]G. G. Romero, V. F. Ruíz Ruíz, A. B. Flores, H. P. Toledo Jaldin, A. R. Vilchis-Nestor, D. M. Ávila-Márquez, D. R. Contreras, *Biocatal. Agric. Biotechnol.,* 2025, **64**, 103492.
[77]A. K. Bhardwaj, A. Shukla, S. Maurya, S. C. Singh, K. N. Uttam, S. Sundaram, M. P. Singh, R. Gopal, *J. Photochem. Photobiol. B: Biol.,* 2018, **188**, 42-49.
[78]L. Colleselli, M. Mutschlechner, M. Spruck, F. Albrecht, O. I. Strube, P. Vrabl, S. Zeilinger, H. Schöbel, *Bioprocess Biosyst. Eng.,* 2024, **47**, 1669-1682.
[79]M. Fahim, A. Shahzaib, N. Nishat, A. Jahan, T. A. Bhat, A. Inam, *JCIS Open,* 2024, **16**, 100125.
[80]S. A. Lawrence, *Amines: Synthesis, Properties and Applications*, Cambridge University Press, New York, **2004**.
[81]L.-Y. Liang, Y.-H. Kung, V. K. S. Hsiao, C.-C. Chu, *Nanomaterials,* 2023, **13**.
[82]A. Mahata, R. K. Rai, I. Choudhuri, S. K. Singh, B. Pathak, *Phys. Chem. Chem. Phys.,* 2014, **16**, 26365-26374.
[83]S. Doherty, J. G. Knight, T. Backhouse, R. J. Summers, E. Abood, W. Simpson, W. Paget, R. A. Bourne, T. W. Chamberlain, R. Stones, K. R. J. Lovelock, J. M. Seymour, M. A. Isaacs, C. Hardacre, H. Daly, N. H. Rees, *ACS Catal.,* 2019, **9**, 4777-4791.
[84]G.-B. Wang, K.-H. Xie, J.-L. Kan, H.-P. Xu, F. Zhao, Y.-J. Wang, Y. Geng, Y.-B. Dong, *Chem. Commun.,* 2023, **59**, 1493-1496.
[85]H. Bao, L. Wang, *Org. Lett.,* 2023, **25**, 8872-8876.
[86]C. Gao, Q. Xuan, Q. Song, *Chin. J. Chem.,* 2021, **39**, 2504-2508.

View Article Online
DOI: 10.1039/D6NA00170J

Data availability

The data supporting this article has been included as part of the supplementary information (SI). Supplementary information: Spectroscopic studies of stabilizers, amount of photocatalyst, sacrificial electron donors, thermodynamic studies and copies of ^{1}H and ^{13}C NMR spectra of synthesized anilines (2). See DOI: DOI: 10.1039/x0xx00000x